BIOCHEMISTRY
including biophysical chemistry & molecular biology

Article

pubs.acs.org/biochemistry

Molecular Basis for the Substrate Stereoselectivity in Tryptophan Dioxygenase

Luciana Capece,[†] Ariel Lewis-Ballester,[‡] Marcelo A. Marti,[†,§] Dario A. Estrin,*[,†] and Syun-Ru Yeh*[,‡]

[†]Departamento de Química Inorgánica, Analítica y Química Física/INQUIMAE-CONICET Facultad de Ciencias Exactas y Naturales, Universidad de Buenos Aires, Ciudad Universitaria, Pabellón 2, Buenos Aires C1428EHA, Argentina

[‡]Department of Physiology and Biophysics, Albert Einstein College of Medicine, 1300 Morris Park Avenue, Bronx, New York 10461, United States

[§]Departamento de Química Biológica, Facultad de Ciencias Exactas y Naturales, Universidad de Buenos Aires, Ciudad Universitaria, Pabellón 2, Buenos Aires C1428EHA, Argentina

Supporting Information

ABSTRACT: Tryptophan dioxygenase (TDO) and indoleamine 2,3-dioxygenase (IDO) are the only two heme proteins that catalyze the oxidation reaction of tryptophan (Trp) to *N*-formylkynurenine. While human IDO is able to oxidize both L- and D-Trp, human TDO (hTDO) displays major specificity for L-Trp. In this work, we aim to interrogate the molecular basis for the substrate stereoselectivity of hTDO. Our previous molecular dynamics simulation studies of *Xanthomonas campestris* TDO (xcTDO) showed that a hydrogen bond between T254 (T342 in hTDO) and the ammonium group of the substrate is present in the L-Trp-bound enzyme, but not in the D-Trp-bound enzyme. The fact that this is the only notable structural alteration induced by the change in the stereo structure of the substrate prompted us to produce and characterize the T342A mutant of hTDO to evaluate the structural role of T342 in controlling the substrate stereoselectivity of the enzyme. The experimental results indicate that the mutation only slightly perturbs the global structural properties of the enzyme but totally abolishes the substrate stereoselectivity. Molecular dynamics simulations of xcTDO show that T254 controls the substrate stereoselectivity of the enzyme by (i) modulating the hydrogen bonding interaction between the NH_3^+ group and epoxide oxygen of the ferryl−indole 2,3-epoxide intermediate of the enzyme and (ii) regulating the dynamics of two active site loops, $loop_{250-260}$ and $loop_{117-130}$, critical for substrate binding.

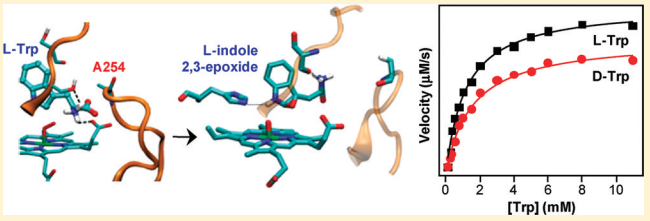

Tryptophan dioxygenase (TDO) is a heme-containing enzyme that catalyzes the conversion of L-tryptophan (L-Trp) to *N*-formylkynurenine (NFK), which represents the first and rate-limiting step of the L-Trp catabolism through the kynurenine pathway.[1] TDO is a ubiquitous enzyme found in bacteria, insects, and mammals. In mammals, it is expressed mainly in the liver, where it is responsible for L-Trp processing that ultimately leads to the biosynthesis of NAD and NADP.[2,3]

Indoleamine 2,3-dioxygenase (IDO) is also a heme-containing enzyme that catalyzes the same oxidation reaction of L-Trp. Contrary to TDO, in mammals IDO is expressed in all tissues other than the liver. Recently, significant efforts to unravel the reaction and inhibition mechanisms of IDO and TDO have been undertaken, as promoted by the discovery that IDO plays a pivotal role in cancer immune escape.[4−8] Along this line, it has been demonstrated that the combination of an IDO inhibitor, 1-methyl-Trp, and cytotoxic chemotherapy leads to significant tumor regression in mouse model systems.[4] In this context, it is important to develop potent IDO inhibitors that do not interfere with normal TDO function.

The crystal structure of mammalian TDO is not known; nonetheless, those of two bacterial isoforms of TDO, from *Xanthomonas campestris* [xcTDO, Protein Data Bank (PDB) entry 2NW8][9] and *Ralstonia metallidurans* (rmTDO, PDB entry 2NOX),[10] were published in 2007. In the case of xcTDO, the enzyme was crystallized in both substrate-free and L-Trp-bound forms. In the structure of the L-Trp-bound form, several tight contacts between L-Trp and the enzyme are evident (Figure 1), including H-bonding interactions between the carboxylate group of L-Trp and Y113/R117, the ammonium group of L-Trp, T254 and the propionate A group of the heme, and the indoleamine group of L-Trp and H55, as well as the hydrophobic interactions among L-Trp, F51, L120, and F116 (F116 is not shown in Figure 1 for the sake of clarity). Structure-based sequence alignment data suggest that most of the key interactions between the substrate and the enzyme observed in xcTDO are conserved in human IDO (hIDO).[9,11,12] Consistently, our hybrid quantum mechanics and molecular mechanics (QM−MM) studies[13,14] showed that xcTDO and hIDO conduct the Trp dioxygenation reaction with a similar ferryl-based mechanism. On the basis of this mechanism, the heme iron-bound dioxygen is first inserted into

Received: September 15, 2011
Revised: November 14, 2011
Published: November 14, 2011

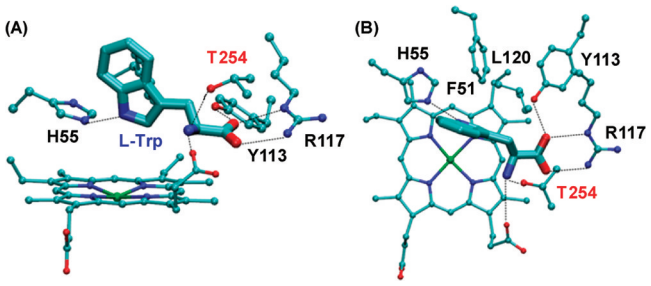

Figure 1. Frontal (A) and top (B) views of the active site of L-Trp-bound xcTDO.[9] The key residues stabilizing the bound L-Trp are highlighted and labeled in black and red.

the C_2 atom of Trp to generate a ferryl−indole 2,3-epoxide intermediate. The subsequent ring-opening reaction of the epoxide, catalyzed by the transfer of a proton from the ammonium group to the epoxide, triggers the insertion of the ferryl oxygen onto the C_2 atom to generate the NFK product. In this scenario, the proper positioning of the ammonium group of the substrate, as well as the electronic environment surrounding it, is believed to be critical for the catalysis.

Although TDO and IDO exhibit a high degree of structural similarity and follow a similar dioxygenase mechanism, they exhibit several intriguing differences in substrate stereoselectivity. hTDO shows comparable affinities for L-Trp and D-Trp, but the k_{cat} for L-Trp is 10-fold higher than that of D-Trp;[12] in contrast, hIDO displays an ∼170-fold higher affinity for L-Trp than for D-Trp,[15] but the k_{cat} values are similar for the two stereoisomers. The structural factors leading to the differences in the substrate stereoselectivity of the two enzymes are unclear. Nonetheless, our previous molecular dynamics (MD) simulation data[16] suggest that most of the interactions between the substrate and the enzyme in xcTDO are conserved in the L-Trp- and D-Trp-bound complexes, except that the strong H-bond between the ammonium group of L-Trp and the OH group of T254 (equivalent to T342 in hTDO) is significantly weakened in the D-Trp-bound enzyme, implying that T254 plays a critical role in controlling the substrate stereoselectivity of xcTDO.

To define the role of T342 in the substrate stereoselectivity of hTDO, we have produced and characterized the T342A mutant by using resonance Raman and optical absorption spectroscopies and determined its activity toward L-Trp and D-Trp. Our data show that the T342A mutation causes only minor changes to the global structure of the enzyme but totally abolishes the substrate stereoselectivity. To unveil the structural perturbations to the enzyme underlying its lack of substrate stereoselectivity, the experimental work was complemented with classical MD simulations. As the crystal structure of hTDO is not available, the simulations were conducted with xcTDO. The simulation data of the L- and D-Trp-bound O_2 complexes, as well as the corresponding ferryl−indole 2,3-epoxide intermediates, indicate that T254 controls the substrate stereoselectivity of xcTDO by modulating the H-bonding interaction between the ammonium group and the epoxide oxygen of the ferryl−indole 2,3-epoxide intermediate and by regulating the interactions between two critical loops, $loop_{250-260}$ and $loop_{117-130}$, that sequester substrate in the active site.

MATERIALS AND METHODS

Expression and Purification of Wild-Type hTDO. The details of protein expression and purification are described elsewhere.[12,17] Briefly, the hTDO protein, with N- and C-terminal tails truncated, and a six-His tag extension at the C-terminus, was overexpressed in *Escherichia coli* BL21 Star(DE3) cells by using the pET30b vector (Stratagene, La Jolla, CA). The transformant was selected from a single colony on an LB kanamycin agar plate and was used to inoculate LB medium, supplemented with 50 μg/mL kanamycin. This starter culture was grown overnight at 37 °C and was subsequently used to inoculate 1 L of LB medium. The resulting *E. coli* culture was grown at 37 °C in a shaker at 250 rpm until the optical density at 600 nm reached ∼0.8. The expression of hTDO was induced by isopropyl β-D-1-thiogalactopyranoside (IPTG), with a final concentration of 1 mM. An aliquot of hemin, with a final concentration of 8−10 μM, was added to the culture to ensure the complete incorporation of the heme prosthetic group into the recombinant protein. The culture was grown at 25 °C for an additional 6−8 h in a shaker at 150 rpm. The cells were harvested by centrifugation and stored at −20 °C until they were used.

The recombinant protein was purified by affinity chromatography with a Ni-NTA column (Novagen). The protein was eluted with 250 mM imidazole (Sigma) in 50 mM phosphate buffer (pH 7.8) and 250 mM KCl. To stabilize the protein, 10 mM L-Trp and 5% glycerol were present throughout the purification procedure. To ensure that the protein was in its ferric state, it was oxidized with potassium ferricyanide and subsequently passed through a Sephadex G25 column to remove the ferricyanide, L-Trp, imidazole, and glycerol. The purity of the protein was confirmed by sodium dodecyl sulfate−polyacrylamide gel electrophoresis (SDS−PAGE) analysis as shown in Figure S2 of the Supporting Information. The protein thus collected was stored in 100 mM phosphate buffer (pH 7.5) with 150 mM KCl at −80 °C until use.

The T342A mutant was created by using the QuikChange II kit (Stratagene) with the following primers: 5′-CAG-CAAAGCTGGCGCCGGTGGTTCCTC-3′ (sense primer) and 5′-GAGGAACCACCGGCGCCAGCTTTGCTG-3′ (anti-sense primer). The sequence was verified by DNA sequence analysis. The mutant was cloned, expressed, and purified by using the same protocol described for the wild-type protein.

Steady-State Activity Assay. For the activity assay, the ferric hTDO was rapidly mixed with sodium ascorbate (100-fold excess with respect to the protein) in the presence of the desired amount of L-Trp in pH 7.0 phosphate buffer (100 mM). The temperature was controlled with a water bath at 25 °C. The final concentration of hTDO was 0.5 μM. The reaction rate was followed by monitoring product formation at 321 nm (ε = 3750 M^{-1} cm^{-1} for *N*-formylkynurenine).[12,18] Two representative kinetic traces obtained with 8 mM L- and D-Trp are shown in Figure S3 of the Supporting Information. The initial product formation rate was plotted as a function of L-Trp concentration; the data were analyzed by Michealis−Menten curve fitting with Origin version 6.1 (Microcal Software, Inc.).

Spectroscopic Measurements. The optical absorption spectra were recorded on a spectrophotometer, UV2100, from Shimadzu Scientific Instruments, Inc. (Columbia, MD), with a spectral slit width of 1 nm. The resonance Raman spectra were recorded on the instrument described previously.[19] Briefly, the 413.1 nm excitation from a Kr ion laser (Spectra Physics,

dx.doi.org/10.1021/bi201439m | *Biochemistry* 2011, 50, 10910−10918

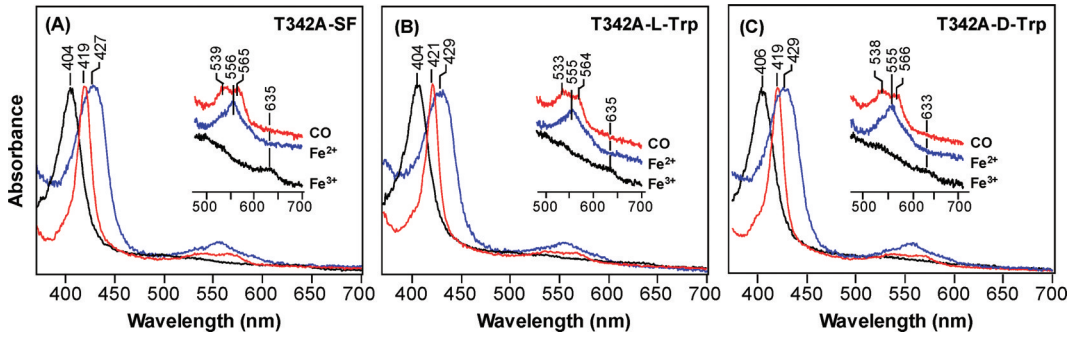

Figure 2. Optical absorption spectra of the T342A mutant of hTDO in the substrate-free form (SF) (A), L-Trp-bound form (B), or D-Trp-bound form (C). Results for the ferric, ferrous, and CO-bound forms are presented in black, blue, and red, respectively. All the spectral intensities are normalized to the Soret band.

Mountain View, CA) was focused to a 30 μm spot on a spinning quartz cell rotating at 1000 rpm. The scattered light, collected at a right angle to the incident laser beam, was focused on the 100 μm wide entrance slit of a 1.25 m Spex spectrometer equipped with a 1200 grooves/mm grating (Horiba Jobin Yvon, Edison, NJ), where it was dispersed and then detected by a liquid nitrogen-cooled CCD detector (Princeton Instruments, Trenton, NJ). A holographic notch filter (Kaiser, Ann Arbor, MI) was used to remove the laser line. The Raman shift was calibrated by using indene (Sigma) as a reference. The laser power was kept at ~5 mW for all measurements, except that used for the CO complexes, for which it was kept at <1 mW to avoid photodissociation of the heme-bound CO. The acquisition time was 30 min for all but the super high-frequency spectra of the CO-bound complexes, for which the acquisition time was 180 min. The ferrous derivative was prepared by reducing the ferric protein, prepurged with N_2 gas, with sodium dithionite under anaerobic conditions. The CO-bound ferrous complexes were obtained by a gentle purging with CO gas on the surface of the solution containing the ferrous form of the enzyme under anaerobic conditions. The concentration of the protein samples used for the Raman measurements was 50 μM in pH 7.0 phosphate buffer (100 mM).

Starting Structures for Classical Molecular Dynamics Simulations. Because of the fact that the crystal structure of hTDO is not available, we have performed the simulations on the xcTDO structure. Sequence comparison of hTDO and xcTDO with seven other TDOs from various organisms (Figure S1 of the Supporting Information) indicates that most of the residues involved in Trp binding are conserved, including H76 (55 in xcTDO), R144 (117 in xcTDO), F72 (51 in xcTDO), F143 (116 in xcTDO), and L147 (120 in xcTDO), with the exception of Y113 of xcTDO that is replaced with a Phe in all the analyzed mammalian and insect sequences. Additionally, $loop_{250-260}$ and $loop_{117-130}$ involved in the observed conformational change in the T254A mutant of xcTDO display a high degree of sequence homology, with all relevant residues involved in the interactions conserved. In this context, the structure of xcTDO provides a good model of the human protein, justifying its use for the MD simulations.

The structure of the ternary complex of xcTDO was based on the crystal structure of the ferrous L-Trp-bound xcTDO (PDB entry 2NW8),[9] as described previously.[13,16] Briefly, a one-subunit model of xcTDO was constructed by removal of residues E19−S35 from subunit A and addition of residues R21−S35 of subunit B, which corresponds to a short helix that penetrates into the structure of the A subunit. The structure of D-Trp-bound xcTDO was obtained by a docking protocol described in ref 16. The structure of the ferryl−L- or D-indole 2,3-epoxide intermediate of xcTDO was obtained from the QM−MM simulations of the corresponding ternary complexes.[13,20] Starting from the structures of the ternary complexes and the ferryl−indole 2,3-epoxide intermediates of the wild-type enzyme, we constructed the corresponding T254A mutant derivatives in silico. These structures were used for all the MD simulations.

Classical Molecular Dynamics Simulations. The starting structure for each complex was immersed in a pre-equilibrated octahedral box of TIP3P water molecules. The standard protonation state at physiological pH was assigned to ionizable residues. Special attention was paid to the protonation states of histidines, which were assigned on the basis of the H-bonding patterns with neighboring residues. All simulations were performed at 300 K and a pressure of 1 bar using a Berendsen thermostat and barostat.[21] Periodic boundary conditions and Ewald sums (grid spacing of 1 Å) were used to treat long-range electrostatic interactions. The SHAKE algorithm was used to keep bonds involving hydrogen atoms at their equilibrium length. A 2 fs time step was used for the integration of Newton's equations. The Amber ff99SB force field[22] was used for all residues but the heme, whose parameters were developed and thoroughly tested previously by our group.[23,24] The parameters for the ferryl−indole 2,3-epoxide intermediate were obtained using standard Amber procedures, using ab initio HF calculations and the RESP[22] method for determining the partial charges. All simulations were performed with the PMEMD module of the AMBER9 package.[25] Equilibration consisted of an energy minimization of the initial structures, followed by a slow heating to 300 K. For each structure, 20 ns MD production runs were performed. Frames were collected at 2 ps intervals, which were subsequently used to analyze the trajectories. Finally, to estimate the work required to produce the rotation of the $C_\alpha-C_\beta$ bond in the ferryl−indole 2,3-epoxide intermediate of the wild type and T254A mutant of xcTDO and make a rough estimation of the free energy profile for the interconversion of the two extreme structures, we added a time-dependent potential that moves the system from the initial to the final configuration, resulting in the equation $E'(r) = E(r) + k[(\xi - \xi_o)^2]$.[26] The constant k was 200 kcal mol^{-1} K^{-1} in all cases, and the coordinate ξ was chosen as the $N-C_\alpha-C_\beta-C_\gamma$ dihedral angle of the epoxide adduct (Figure S9 of the Supporting Information).

Table 1. ν_{Fe-His}, ν_{Fe-CO}, and ν_{C-O} Modes (cm^{-1}) and Electronic Transition Bands (nm) of the Ferric, Ferrous, and CO-Bound Ferrous Derivatives of the Wild Type and T342A Mutant of hTDO in the Substrate-Free (SF), L-Trp-Bound, and D-Trp-Bound Forms

hTDO		ν_{Fe-His}	ν_{Fe-CO}	ν_{C-O}	A_{ferric}	$A_{ferrous}$	A_{CO}	ref
wild type	SF	229	496	1958	406	432	420	12
					633	556	538, 568	
	with L-Trp	229	488	1972	407	433	421	12
						555	537, 567	
	with D-Trp	228	490	nd[a]	406	432	421	12
						558	569	
T342A	SF	227	495	1963	404	427	419	
					635	556	539, 565	
	with L-Trp	227	488	1971	404	429	421	
					635	555	533, 564	
	with D-Trp	227	488	nd[a]	406	429	419	
					633	555	538, 566	

[a]Not determined.

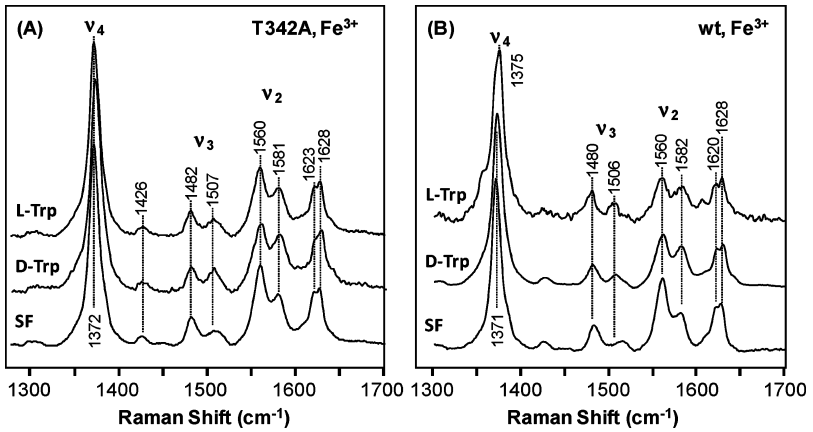

Figure 3. Resonance Raman spectra of the ferric derivative of T342A mutant (A) and wild-type (B) hTDO in the substrate-free (SF), L-Trp-bound, or D-Trp bound form. The spectra of the SF and L-Trp-bound forms of the wild-type enzyme were taken from ref 12. The Trp concentration used for generating the substrate-bound enzyme was 20 mM.

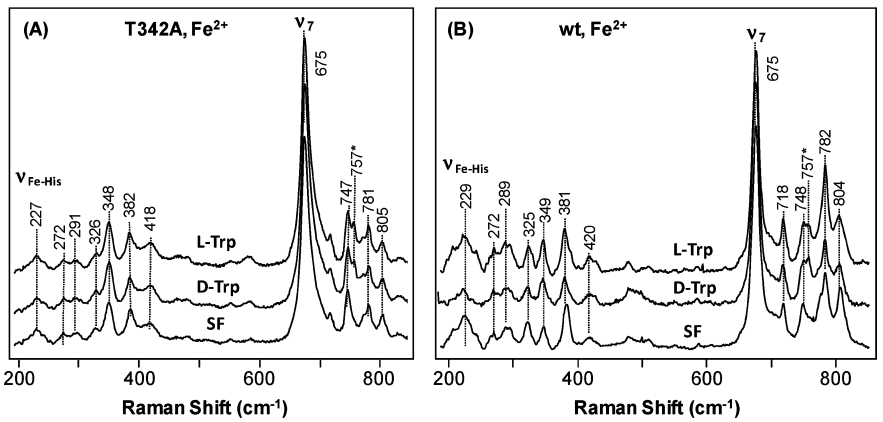

Figure 4. Resonance Raman spectra of the ferrous derivative of T342A mutant (A) and wild-type (B) hTDO, in the substrate-free (SF), L-Trp-bound, or D-Trp bound form. The spectra of the SF and L-Trp-bound forms of the wild-type enzyme were taken from ref 12. The Trp concentration used for generating the substrate-bound enzyme was 20 mM. The peak at 757 cm^{-1} denoted with an asterisk is derived from the Trp substrate.

RESULTS AND DISCUSSION

Optical Absorption and Resonance Raman Spectra of the T342A Mutant of hTDO. Figure 2 shows the optical absorption spectra of the T342A mutant in the absence and presence of L-Trp. In the substrate-free form, the spectra of ferric T342A show a Soret band at 404 nm and a charge transfer band at 635 nm, characteristic of a six-coordinate (6C) water-bound ferric heme, similar to that reported for the wild-type enzyme.[12] The ferrous derivative has a Soret band at 427 nm and a visible band at 556 nm, consistent with a five-coordinate (5C) high-spin heme. The CO-bound complex, on the other hand, shows a Soret band at 419 nm and two visible

dx.doi.org/10.1021/bi201439m | Biochemistry 2011, 50, 10910–10918

bands at 539 and 565 nm, confirming the presence of a 6C low-spin heme. Like that with the wild-type enzyme, the addition of L-Trp or D-Trp to the mutant does not introduce significant modifications into the spectra, as summarized in Table 1.

The resonance Raman spectra of the ferric derivatives of the T342A mutant are shown in Figure 3A. The substrate-free enzyme has a ν_4 mode at 1372 cm^{-1}, ν_2 modes at 1560 and 1581 cm^{-1}, and ν_3 modes at 1482 and 1507 cm^{-1}, indicating a 6C high-spin/low-spin mixed configuration, in good agreement with a water-bound ferric heme, as indicated by the optical absorption spectral data. The addition of L-Trp or D-Trp to the ferric enzyme does not perturb the spectral feature, except that the low-spin component is slightly increased, similar to that observed in the wild-type enzyme (Figure 3B).

The ferrous derivative of the T342A mutant exhibits ν_3 and ν_4 modes at 1470 and 1355 cm^{-1}, respectively, in the absence of substrate, indicating a 5C high-spin heme (data not shown), the same as the reported data for the wild-type enzyme.[12] In the low-frequency window of the spectrum, the Fe–His stretching mode (ν_{Fe-His}) is identified at 227 cm^{-1} (Figure 4A), similar to that of the wild-type enzyme (Figure 4B and Table 1),[12] indicating that the mutation does not perturb the proximal heme environment. Nonetheless, the relative intensities of several in-plane and out-of-plane heme modes in the 250–450 and 700–800 cm^{-1} regions of the spectrum[17,20] are significantly perturbed by the mutation, suggesting conformational changes to the heme prosthetic group due to the mutation. L-Trp or D-Trp binding to the mutant does not introduce noticeable changes into the spectrum, in contrast to the small changes observed for the wild-type enzyme (Figure 4B), manifesting slightly weaker substrate–enzyme interactions in the mutant enzyme.

CO has been demonstrated to be a useful probe for investigating the active site structure of heme proteins. The spectral features of the CO complex of the T342A mutant (Figure S4 of the Supporting Information) are similar to those reported for the wild-type enzyme[12] and are not affected by the addition of L-Trp or D-Trp, except that the Fe–CO stretching mode (ν_{Fe-CO}) at 495 cm^{-1} found in the substrate-free enzyme shifted to 488 cm^{-1} in response to L-Trp or D-Trp binding. The assignments of the ν_{Fe-CO} modes at 495 and 488 cm^{-1}, along with those of the associated C–O stretching modes (ν_{C-O}) at 1963 and 1970 cm^{-1}, were confirmed by $^{12}CO-^{13}CO$ isotope substitution experiments (inset in Figure S4 of the Supporting Information). As listed in Table 1, in general, all the spectral features, as well as their responses to substrate binding, of the various derivatives of the T342A mutant are similar to those reported for the wild-type enzyme,[12] confirming that the mutation does not introduce major structural modifications into the enzyme.

Activity of the T342A Mutant of hTDO toward L- and D-Trp. To determine how the T342A mutation affects the enzyme activity, NFK production activities of the wild type and T342A mutant were followed as a function L-Trp or D-Trp concentration. As shown in Figure 5B, the activity of the wild-type enzyme toward either L-Trp (black symbols) or D-Trp (red symbols) follows typical Michaelis–Menten behavior with k_{cat} and K_m values of 2.24 ± 0.08 s^{-1} and 0.12 ± 0.02 mM or 0.20 ± 0.06 s^{-1} and 0.26 ± 0.02 mM, respectively. The k_{cat} and K_m values are similar to those reported previously (2.1 s^{-1} and 0.19 mM or 0.2 s^{-1} and 0.18 mM for L-Trp or D-Trp, respectively);[12] the small differences are plausibly a result of the slight difference in the experimental temperatures, as the current data

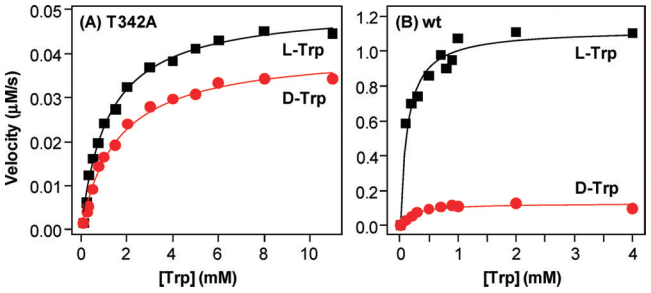

Figure 5. Michaelis–Menten plots of T342A mutant (A) and wild-type (B) hTDO. The black and red symbols were obtained by using L-Trp and D-Trp as the substrate, respectively. The solid lines are best fits of the data to the Michaelis–Menten equation. The best fitted parameters are listed in Table 2. The enzyme concentration used for the measurements was 0.5 μM.

were obtained at 25 °C while the previously reported data were acquired at ambient temperature. The data indicate that hTDO exhibits similar affinity for L-Trp and D-Trp, but the k_{cat} for L-Trp is much higher than that for D-Trp. The T342 mutation leads to the elevation of the K_m values to 1.19 ± 0.09 and 1.59 ± 0.13 mM for L-Trp and D-Trp, respectively (Figure 5A); at the same time, the k_{cat} values are reduced to 0.101 ± 0.002 and 0.082 ± 0.002 s^{-1}, respectively. As listed in Table 2, the T432A

Table 2. Michaelis–Menten Parameters of the Wild Type and T342A Mutant of hTDO[a]

hTDO	substrate	K_m (mM)	k_{cat} (s^{-1})	k_{cat}/K_m
wild type	L-Trp	0.12 ± 0.02	2.24 ± 0.08	18.7
	D-Trp	0.20 ± 0.06	0.26 ± 0.02	1.3
T342A	L-Trp	1.19 ± 0.09	0.101 ± 0.002	0.08
	D-Trp	1.59 ± 0.13	0.082 ± 0.002	0.05

[a]All parameters are taken from the data presented in Figure 5.

mutation results in a similar reduction (~10-fold) in the substrate affinity for L-Trp and D-Trp, but it leads to a much greater reduction in k_{cat} for L-Trp (~20-fold) as compared to D-Trp (~3-fold), indicating the abolishment of substrate stereoselectivity (as manifested by the similar k_{cat} and K_m values of the mutant for the two stereoisomers). Taken together, the data confirm that T342 plays a pivotal role in controlling the substrate stereoselectivity of hTDO.

Molecular Dynamics Simulations of the Ternary Complex of xcTDO. To understand the molecular basis for the abolished substrate stereoselectivity in the T342A mutant of hTDO, we performed 20 ns MD simulations of the ternary complex of the T254A mutant of xcTDO (equivalent to the T342A mutant of hTDO), in which O_2 and Trp were bound to the active site. The data show that the structures of both the L- and D-Trp-bound complexes remained stable during the 20 ns simulations, with a root-mean-square deviation (rmsd) of <2.5 Å with respect to the initial structure (Figures S5 and S6 of the Supporting Information). In addition, the final averaged structures of the mutant show rmsd values of 1.14 and 1.27 Å with respect to the L- and D-Trp-bound wild-type enzyme, respectively, indicating that the mutation does not introduce global structural changes into the enzyme, consistent with the conclusion drawn from the aforementioned spectroscopic studies.

Visual inspection of the obtained MD trajectories, however, revealed important structural differences in the H-bonding

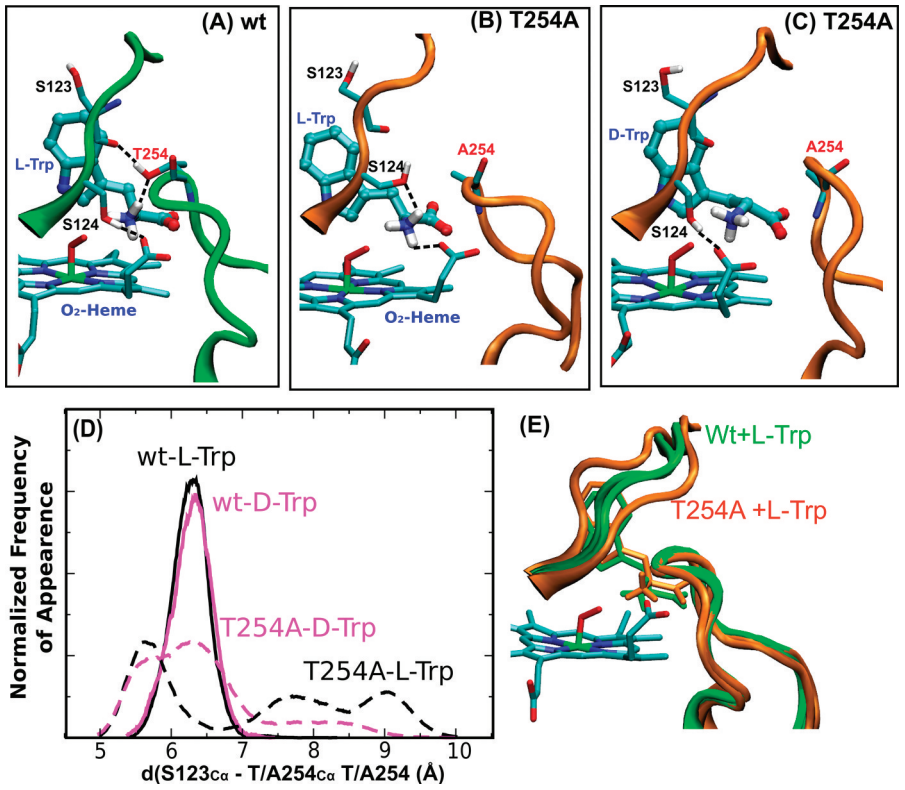

Figure 6. Comparison of the active site structures of the ternary complex of wild-type (A) and T254A mutant (B and C) xcTDO, obtained from MD simulations. (D) Histogram of the $loop_{250-260}$–$loop_{117-130}$ separation, defined by the distance between the C_α atom of S123 and the C_α atom of T/A254, obtained from MD simulations. The data associated with L- and D-Trp-bound complexes are labeled in black and magenta, respectively; those associated with the wild type and T254A are depicted with solid and dashed lines, respectively. (E) Two superimposed extreme structures of the ternary complex of the wild type (labeled in green) and T254A mutant (labeled in orange) of xcTDO, in which the $loop_{250-260}$–$loop_{117-130}$ separations are maximal and minimal.

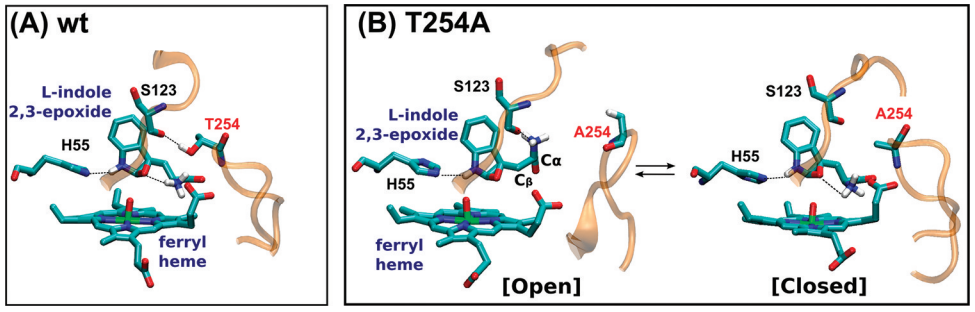

Figure 7. Representative snapshots of the ferryl–L-indole 2,3-epoxide intermediate of wild-type (A) and T254A (B) xcTDO obtained from MD simulations.

network surrounding the NH_3^+ group of the substrate. In the L-Trp-bound wild-type enzyme, the substrate forms strong H-bonds with its surrounding environment, including (1) the indoleamine group and H55, (2) the COO^- group and the side chain groups of Y113 and R117, and (3) the NH_3^+ group, the OH group of T254, the propionate A group of the heme, and the OH group of S124 (Figure 6A). The replacement of L-Trp with D-Trp leads to the interruption of the interaction between the NH_3^+ group and T254, while the rest of the H-binding interactions remain almost the same. It is important to note that T254 and S124 are located in two loop regions that are held close together by an H-bond between the OH group of T254 and the backbone carbonyl group of S123 (Figure 6A). For the sake of clarity, the two loops are denoted as $loop_{250-260}$ and $loop_{117-130}$, respectively, hereafter.

In the L-Trp-bound complex of the T254A mutant, the elimination of the H-bond between the NH_3^+ group of the substrate and T254 leads to only subtle modifications in the H-bonding interactions with H55, Y113, and R117. However, it significantly increases the frequency of the fluctuations of $loop_{250-260}$ (Figure 6E), as evident in the much wider distance distribution of the A254–S123 pair (Figure 6D). The opening of the two loops results in a dynamic distal pocket with fluctuating interactions between the NH_3^+ group of the substrate and its surroundings. In addition, the OH group of S124 rotates to form an H-bond with the NH_3^+ group, instead of the heme propionate A (Figure 6B vs Figure 6A). When the L-Trp is replaced with D-Trp in the mutant complex, the opening of the two loops was also observed (Figure 6D); in

dx.doi.org/10.1021/bi201439m | *Biochemistry* 2011, 50, 10910–10918

addition, heme propionate A forms an H-bond with S124, instead of the NH_3^+ group (Figure 6C vs Figure 6B).

Molecular Dynamics Simulations of the Ferryl−Indole 2,3-Epoxide Intermediate of xcTDO. To gain insight into the role of T254 in controlling catalysis, we performed 20 ns MD simulations of the recently characterized ferryl−indole 2,3-epoxide intermediate of wild-type xcTDO.[14,27] The data show that both the complexes with the L and D isomers remained stable during the 20 ns simulation, showing an rmsd of <2.5 Å (Figures S7 and S8 of the Supporting Information). In the previous studies, we showed that, in the intermediate, the NH_3^+ group forms a strong H-bond with the epoxide oxygen (Figure 7A). This H-bond was shown to be critical for triggering the ring-opening reaction of the epoxide that ultimately leads to product formation.[14,28] As observed in the ternary complex, in the epoxide intermediate of the wild-type enzyme the NH_3^+ group is held in position by H-bonding to heme propionate A and T254; in addition, $loop_{250-260}$ and $loop_{117-130}$ are held together by an H-bond between T254 and S123 (denoted as the "closed" conformation hereafter) (Figure 7A). When L-indole 2,3-epoxide is replaced with the D isomer, the H-bond between T254 and S123 is ruptured during the simulation, allowing the separation of the two loops (denoted as the "open" conformation hereafter). Moreover, a spontaneous rotation of the $C_\alpha-C_\beta$ bond of the epoxide intermediate brings the NH_3^+ group to a new position, thereby temporarily interrupting its H-bonding interaction with the epoxide.

In the ferryl−L-indole 2,3-epoxide intermediate of T254A, the structure fluctuates between the open and closed conformations (Figure 7B) because of the absence of the H-bond between T254 and S123. When the L-indole 2,3-epoxide was replaced with the D isomer, only open conformation was observed. In the open conformation of both L and D isomers, the H-bond between the NH_3^+ group and epoxide is broken, again because of the spontaneous rotation of the $C_\alpha-C_\beta$ bond. Additional calculations show that the estimated free energy barrier for the rotation of the $C_\alpha-C_\beta$ bond in the L-indole 2,3-epoxide intermediate of the wild-type enzyme is very high (~39 kcal/mol), as a result of steric hindrance (Figure S9 of the Supporting Information). The steric hindrance is significantly reduced (~3 kcal/mol) for the D isomer and becomes barrierless for both isomer complexes of the T254A mutant (Figure S9 of the Supporting Information). Finally, we performed additional 6 ns MD simulations of the open conformations of the L and D intermediate of the wild type and T254A mutant, without restraints. It was found that, in the L-indole 2,3-epoxide intermediate of the wild-type enzyme, the NH_3^+ group returned back to its initial position spontaneously, while in the three other cases, the NH_3^+ group remained in the open conformation during the time scale of the simulations, confirming that the conversion of the closed conformation to the open conformation removes the steric hindrance, thereby allowing the rotation of the $C_\alpha-C_\beta$ bond.

Mechanistic Implications. The simulation data of the ternary complex of xcTDO (with both L- and D-Trp) showed that the T254A mutation causes the opening of the $loop_{250-260}-loop_{117-130}$ segment, leading to a more dynamic and open distal pocket, accounting for the much lower substrate affinity (i.e., higher K_m) observed in the activity studies (Table 2). On the other hand, the simulation data of the ferryl−L-indole 2,3-epoxide intermediate indicate that the T254A mutation also results in the opening of the $loop_{250-260}-loop_{117-130}$ segment. It leads to local reorganization of the H-bonding interactions surrounding the NH_3^+ group of the substrate, resulting in an open conformation, in which the H-bond between the NH_3^+ group and the epoxide is temporarily lost. As the H-bond is critical for catalyzing the ring-opening reaction of the epoxide during the dioxygenase chemistry,[14,28] the data account for the ~20-fold reduction in the catalytic activity of the enzyme (see k_{cat} in Table 2). A similar result was observed in the complex of the mutant with the D isomer, accounting for the similar k_{cat} values observed for the two stereoisomers (Table 2). Intriguingly, a similar open conformation is observed for the wild-type complex with the D isomer, accounting for its much lower k_{cat} with respect to that of the L isomer, confirming that T254 plays a crucial role in determining the stereoselectivity of xcTDO.

CONCLUSIONS

In the previous work, we have revealed that hTDO exhibits similar affinities for L- and D-Trp, but the k_{cat} for L-Trp is 10-fold higher than that for D-Trp.[12] The mutagenesis and MD simulation data obtained in this work demonstrate the critical role of T342 in hTDO (and the equivalent residue T254 in xcTDO) in controlling substrate binding, as well as substrate stereoselectivity of the enzyme, by modulating the H-bonding interaction between the NH_3^+ group and epoxide oxygen of the ferryl−indole 2,3-epoxide intermediate of the enzyme and by regulating the dynamics of $loop_{250-260}$ and $loop_{117-130}$. The crystallographic structural data show that substrate binding to xcTDO induces the closure and/or organization of the two loops to sequester and stabilize the bound substrate. Sequence alignment along with the structural data of the substrate-free hIDO (the only structure available for hIDO) reveals that the substrate-induced loop closure also occurs in hIDO; in addition, T254 and S124 are fully conserved in hIDO, but S123 is replaced with a Gly.

It is plausible that, because of the absence of the T254−S123 interaction, hIDO displays an ~170-fold higher affinity for L-Trp than for D-Trp, but the k_{cat} values are similar for the two stereoisomers,[12] opposite to what is observed in hTDO. Apparently, T254 (T342) is not the only player in determining the substrate stereoselectivity of TDO; we are in a process of evaluating the role of S123 in the stereoselectivity of xcTDO. In any case, the mutagenesis results presented here agree perfectly with the prediction made in our previous work, in which T254 in xcTDO was identified as one of the key residues for controlling the stereoselectivity of the enzyme. In this sense, our new experimental work validates the computational methodology and confirms the predictive power of this tool.

ASSOCIATED CONTENT

Supporting Information

Sequence alignment of various isoforms of TDO, SDS−PAGE data of the T324 mutant, kinetic trances for formation of the product from the T254A mutant, resonance Raman spectra for the Trp−CO complexes of xcTDO, rmsd and potential energy of the Trp−O_2 complexes and ferryl−L-indole 2,3-epoxide intermediates of xcTDO as a function of MD simulation time, and calculated work required for the transition between the closed and open conformations of the ferryl−L-indole 2,3-epoxide intermediate of xcTDO. This material is available free of charge via the Internet at http://pubs.acs.org.

AUTHOR INFORMATION

Corresponding Author

*D.A.E.: e-mail, dario@qi.fcen.uba.ar; phone, +541145763380; fax, +541145763341. S.-R.Y.: e-mail, syun-ru.yeh@einstein.yu.edu; phone, (718) 430-4234; fax, (718) 430-4230.

Funding

This work was supported by National Institutes of Health Grant GM086482 and National Science Foundation Grant 1026788 to S.-R.Y. and National Institutes of Health Molecular Biophysics Training Grant GM008572 to A.L.-B. It was also partially supported by grants from Universidad de Buenos Aires 08-X625 to M.A.M. and 08-X074 to D.A.E., ANPCYT 07-1650 to M.A.M., and 06-25667 and Conicet PIP 01207 to D.A.E. D.A.E. and M.A.M. are members of CONICET. L.C. thanks CONICET, the Fulbright Foundation, and the Bunge & Born Foundation for the fellowships that allowed her to perform this work.

ACKNOWLEDGMENTS

Computer power was generously provided by Cecar at FCEN, Universidad de Buenos Aires, and Cluster MCG at Universidad Nacional de Córdoba.

ABBREVIATIONS

TDO, tryptophan dioxygenase; IDO, indoleamine 2,3-dioxygenase; hIDO, human IDO; NFK, *N*-formylkynurenine; hTDO, human TDO; rmTDO, *R. metallidurans* TDO; xcTDO, *X. campestris* TDO; MD, molecular dynamics; 6C, six-coordinate; 5C, five-coordinate.

REFERENCES

(1) Sono, M., Roach, M. P., Coulter, E. D., and Dawson, J. H. (1996) Heme-Containing Oxygenases. *Chem. Rev. 96*, 2841−2888.

(2) Takikawa, O. (2005) Biochemical and medical aspects of the indoleamine 2,3-dioxygenase-initiated L-tryptophan metabolism. *Biochem. Biophys. Res. Commun. 338*, 12−19.

(3) Knox, W. E., and Mehler, A. H. (1950) The Conversion of Tryptophan to Kynurenine in Liver: I. The Coupled Tryptophan Peroxidase-Oxidase System Forming Formylkynurenine. *J. Biol. Chem. 187*, 419−430.

(4) Muller, A. J., DuHadaway, J. B., Donover, P. S., Sutanto-Ward, E., and Prendergast, G. C. (2005) Inhibition of indoleamine 2,3-dioxygenase, an immunoregulatory target of the cancer suppression gene Bin1, potentiates cancer chemotherapy. *Nat. Med. 11*, 312−319.

(5) Munn, D. H., Shafizadeh, E., Attwood, J. T., Bondarev, I., Pashine, A., and Mellor, A. L. (1999) Inhibition of T Cell Proliferation by Macrophage Tryptophan Catabolism. *J. Exp. Med. 189*, 1363−1372.

(6) Grohmann, U., Fallarino, F., and Puccetti, P. (2003) Tolerance, DCs and tryptophan: Much ado about IDO. *Trends Immunol. 24*, 242−248.

(7) Friberg, M., Jennings, R., Alsarraj, M., Dessureault, S., Cantor, A., Extermann, M., Mellor, A. L., Munn, D. H., and Antonia, S. J. (2002) Indoleamine 2,3-dioxygenase contributes to tumor cell evasion of T cell-mediated rejection. *Int. J. Cancer 101*, 151−155.

(8) Uyttenhove, C., Pilotte, L., Theate, I., Stroobant, V., Colau, D., Parmentier, N., Boon, T., and Van den Eynde, B. J. (2003) Evidence for a tumoral immune resistance mechanism based on tryptophan degradation by indoleamine 2,3-dioxygenase. *Nat. Med. 9*, 1269−1274.

(9) Forouhar, F., Anderson, J. L. R., Mowat, C. G., Vorobiev, S. M., Hussain, A., Abashidze, M., Bruckmann, C., Thackray, S. J., Seetharaman, J., Tucker, T., Xiao, R., Ma, L.-C., Zhao, L., Acton, T. B., Montelione, G. T., Chapman, S. K., and Tong, L. (2007) Molecular insights into substrate recognition and catalysis by tryptophan 2,3-dioxygenase. *Proc. Natl. Acad. Sci. U.S.A. 104*, 473−478.

(10) Zhang, Y., Kang, S. A., Mukherjee, T., Bale, S., Crane, B. R., Begley, T. P., and Ealick, S. E. (2007) Crystal structure and mechanism of tryptophan 2,3-dioxygenase, a heme enzyme involved in tryptophan catabolism and in quinolinate biosynthesis. *Biochemistry 46*, 145−155.

(11) Sugimoto, H., Oda, S.-i., Otsuki, T., Hino, T., Yoshida, T., and Shiro, Y. (2006) Crystal structure of human indoleamine 2,3-dioxygenase: Catalytic mechanism of O_2 incorporation by a heme-containing dioxygenase. *Proc. Natl. Acad. Sci. U.S.A. 103*, 2611−2616.

(12) Batabyal, D., and Yeh, S. R. (2007) Human Tryptophan Dioxygenase: A Comparison to Indoleamine 2,3-Dioxygenase. *J. Am. Chem. Soc. 129*, 15690−15701.

(13) Capece, L., Lewis-Ballester, A., Batabyal, D., Di Russo, N., Yeh, S. R., Estrin, D. A., and Marti, M. A. (2010) The first step in the dioxygenation reaction carried out by tryptophan dioxygenase and indoleamine 2,3- dioxygenase as revealed by QM-MM studies. *J. Biol. Inorg. Chem. 15*, 811−823.

(14) Capece, L., Lewis-Ballester, A., Yeh, S.-R., Estrin, D. A., and Marti, M. A. (2011) The Complete Reaction Mechanism of Indoleamine 2,3-Dioxygenase As Revealed by QM/MM Simulations. *J. Phys. Chem. B*, manuscript under revision.

(15) Lu, C., Lin, Y., and Yeh, S.-R. (2009) Inhibitory Substrate Binding Site of Human Indoleamine 2,3-Dioxygenase. *J. Am. Chem. Soc. 131*, 12866−12867.

(16) Capece, L., Arrar, M., Roitberg, A. E., Yeh, S.-R., Marti, M. A., and Estrin, D. A. (2010) Substrate stereo-specificity in tryptophan dioxygenase and indoleamine 2,3-dioxygenase. *Proteins: Struct., Funct., Bioinf. 78*, 2961−2972.

(17) Batabyal, D., and Yeh, S.-R. (2009) Substrate-Protein Interaction in Human Tryptophan Dioxygenase: The Critical Role of H76. *J. Am. Chem. Soc. 131*, 3260−3270.

(18) Ishimura, Y., Nozaki, M., Hayaishi, O., Nakamura, T., Tamura, M., and Yamazaki, I. (1970) The Oxygenated Form of L-Tryptophan 2,3-Dioxygenase as Reaction Intermediate. *J. Biol. Chem. 245*, 3593−3602.

(19) Egawa, T., and Yeh, S.-R. (2005) Structural and functional properties of hemoglobins from unicellular organisms as revealed by resonance Raman spectroscopy. *J. Inorg. Biochem. 99*, 72−96.

(20) Lewis-Ballester, A., Batabyal, D., Egawa, T., Lu, C., Lin, Y., Marti, M. A., Capece, L., Estrin, D. A., and Yeh, S. R. (2009) Evidence for a Ferryl Intermediate in Heme-based Dioxygenases: Mechanistic Implications. *Proc. Natl. Acad. Sci. U.S.A. 106*, 17371−17376.

(21) Berendsen, H. J. C., Postma, J. P. M., van Gunsteren, W. F., DiNola, A., and Haak, J. R. (1984) Molecular dynamics with coupling to an external bath. *J. Chem. Phys. 81*, 3684−3690.

(22) Wang, J., Cieplak, P., and Kollman, P. A. (2000) How well does a restrained electrostatic potential (RESP) model perform in calculating conformational energies of organic and biological molecules? *J. Comput. Chem. 21*, 1049−1074.

(23) Marti, M. A., Crespo, A., Capece, L., Boechi, L., Bikiel, D. E., Scherlis, D. A., and Estrin, D. A. (2006) Dioxygen affinity in heme proteins investigated by computer simulation. *J. Inorg. Biochem. 100*, 761−770.

(24) Bidon-Chanal, A., Martí, M. A., Estrin, D. A., and Luque, F. J. (2009) Exploring the nitric oxide detoxification mechanism of mycobacterium tuberculosis truncated haemoglobin N. *NATO Science for Peace and Security Series A: Chemistry and Biology,*, 33−47.

(25) Pearlman, D. A., Case, D. A., Caldwell, J. W., Ross, W. S., Cheatham, T. E., DeBolt, S., Ferguson, D., Seibel, G., and Kollman, P. (1995) AMBER, a package of computer programs for applying molecular mechanics, normal mode analysis, molecular dynamics and free energy calculations to simulate the structural and energetic properties of molecules. *Comput. Phys. Commun. 91*, 1−41.

(26) Marti, M. A., Capece, L., Bidon-Chanal, A., Crespo, A., Guallar, V., Luque, F. J., and Estrin, D. A. (2008) Nitric oxide reactivity with globins as investigated through computer simulation. *Methods Enzymol. 437*, 477−498.

(27) Chung, L. W., Li, X., Sugimoto, H., Shiro, Y., and Morokuma, K. (2008) Density functional theory study on a missing piece in understanding of heme chemistry: The reaction mechanism for

indoleamine 2,3-dioxygenase and tryptophan 2,3-dioxygenase. *J. Am. Chem. Soc. 130*, 12299−12309.
(28) Chung, L. W., Li, X., Sugimoto, H., Shiro, Y., and Morokuma, K. (2010) ONIOM Study on a Missing Piece in Our Understanding of Heme Chemistry: Bacterial Tryptophan 2,3-Dioxygenase with Dual Oxidants. *J. Am. Chem. Soc. 132*, 11993−12005.